Light-Responsive Prodrug-Based Supramolecular Nanosystems for Site-Specific Combination Therapy of Cancer

Soo Zeng Fiona Phua,[†#] Chencheng Xue,[§#] Wei Qi Lim,[‡] Guangbao Yang,[†] Hongzhong Chen,[†] Yuanyuan Zhang,[†] Chintya Fransisca Wijaya,[†] Zhong Luo,[,§] Yanli Zhao*[,†,‡]*

[†]Division of Chemistry and Biological Chemistry, School of Physical and Mathematical Sciences, Nanyang Technological University, 21 Nanyang Link, Singapore 637371, Singapore

[‡]NTU-Northwestern Institute for Nanomedicine, Interdisciplinary Graduate School, Nanyang Technological University, 50 Nanyang Drive, Singapore 637553

[§]Key Laboratory of Biorheological Science and Technology, Ministry of Education, College of Bioengineering, Chongqing University, Chongqing 400044, P. R. China

ABSTRACT. On-demand release of chemotherapeutic drugs from their prodrugs triggered by light irradiation has been attracting great attention for effective cancer treatment. Herein, we prepared prodrug-based supramolecular nanoparticles (HA-aPS-aCPT) composed of (1) β-cyclodextrin conjugated hyaluronic acid polymer (HA-CD), (2) adamantane modified camptothecin prodrug (aCPT) caged *via* reactive oxygen species (ROS) responsive thioketal linker, and (3) adamantane modified photosensitizer (aPS), for combination photodynamic therapy and light-controlled chemotherapy. aCPT could release free camptothecin by the cleavage of ROS sensitive thioketal linker. aPS is employed to produce ROS under light irradiation. HA-aPS-aCPT nanoparticles are formed by supramolecular means with excellent colloidal stability and mono-dispersity in aqueous solution. Confocal imaging and flow cytometric analysis confirm the selective uptake of HA-aPS-aCPT nanoparticles *via* CD44

receptor mediated endocytosis by MDA-MB-231 cells, on account of the targeting capability of hyaluronic acid. Cell viability assays show that HA-aPS-aCPT nanoparticles possess minimal cytotoxicity in the dark, while presenting high cellular toxicity under light irradiation. *In vivo* experiments exhibit selective accumulation of HA-aPS-aCPT nanoparticles in MDA-MB-231 tumor of nude mice. Significant tumor regression is observed when light irradiation is applied after intravenous injection of HA-aPS-aCPT nanoparticles. Thus, HA-aPS-aCPT nanoparticles demonstrate a great potential for on-demand combination photodynamic therapy and chemotherapy of tumor.

Introduction

Prodrugs have been synthesized to overcome various drawbacks of anticancer drugs such as high systemic toxicity.[1] Site-specific on-demand release of bioactive drugs from prodrugs would be useful in mitigating high systemic toxicity.[2,3] Various endogenous stimuli[4] such as low intracellular pH,[5-7] elevated glutathione concentration,[8-10] specific overly expressed enzymes,[11,12] and hypoxia,[13,14] as well as exogenous stimuli such as heat,[15] light,[13,16-20] and ultrasound[21,22] have been developed for on-demand release of active drugs from prodrugs. In particular, exogenous stimuli present an added advantage over their endogenous counterpart because of their independence of varying tumor microenvironment, non-invasiveness and excellent spatiotemporal control.[23] Light as an exogenous stimulus has been widely employed for the controlled release of photocaged prodrugs[20,24] including *o*-nitrophenyl[25,26] and coumarinyl ester.[27] However, the limitation of using these photocages came from low wavelength light used that has intrinsic phototoxicity and limited tissue penetration depth, thereby reducing the treatment efficiency in solid tumors.[25,26,28-30] Current research thus aims to develop

photoactivated prodrugs that release active drugs under light irradiation in red or near infrared (NIR) region.[31-33] For example, Schnermann *et. al.* synthesized antibody-drug conjugates that were selectively cleaved by NIR light on account of the instability of the heptamethine cyanine fluorophore to light.[34-36] Photosensitizers were also conjugated to drugs *via* reactive oxygen species (ROS)-responsive linkers to promote photodynamic therapy (PDT) and subsequent release of free drugs upon light irradiation. Some examples of ROS-responsive linkers include aminoacrylate,[37] thioether,[38,39] diselenide,[40] thioketal,[17] arylboronic ester,[41] and peroxalate ester.[42] Liu *et. al.* developed porphyrin conjugated gemcitabine prodrug through a thioketal linker that is responsive to singlet oxygen ($^1O_2$) for releasing free gemcitabine.[17] Instead of a direct photocleavage of prodrugs, free drugs were released when ROS adducts produced in response to light irradiation reacted with ROS sensitive bonds in these prodrugs.

On the other hand, some prodrugs require complicated synthesis, tedious purifications, poor solubility for *in vivo* applications, and instability when exposed to stimuli such as light for unexpected release of drugs before the administration. Thus, nanoparticles (NPs) incorporating ROS-responsive thioketal linkers were also fabricated to enhance the drug accumulation.[18,19,43,44] For instance, Yue *et. al.* fabricated a mitochondria-targeting system comprising of zinc phthalocyanine and a copolymer modified with triphenylphosphonium as the targeting ligand and camptothecin (CPT) prodrug through a thioketal linker.[18] In another work, Pei *et. al.* fabricated a red-blood cell membrane co-loaded with paclitaxel prodrug and photosensitizers.[45] Although these systems showed enhanced solubility of prodrugs, they had the inflexibility in adjusting the ratio between photosensitizers and drugs. Precise control on the ratio of drugs and photosensitizers would be essential in cancer therapy, since such systems could ensure accurate clinical prescriptions of chemotherapeutic drugs and photosensitizers.

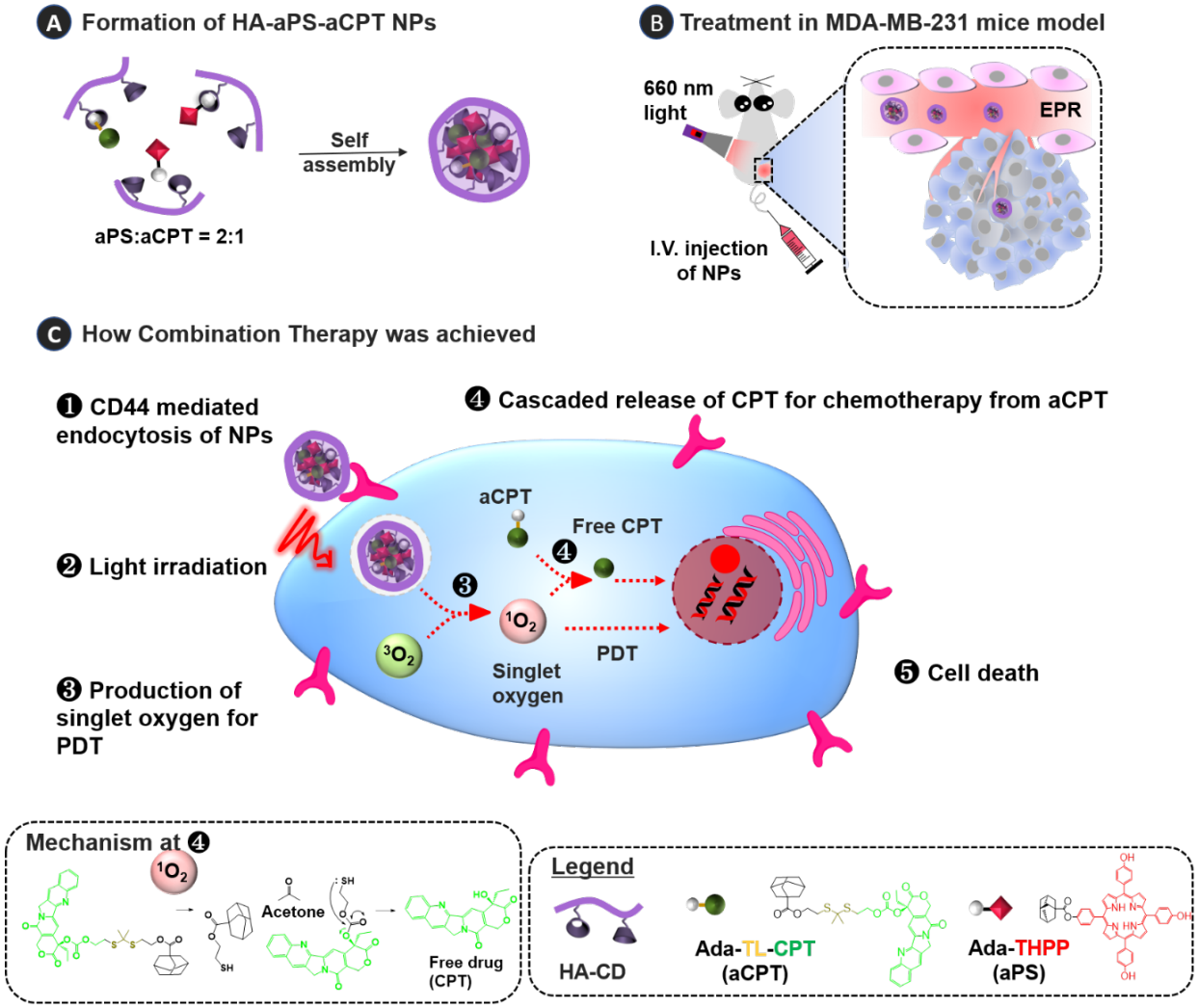

Scheme 1. Schematic representation illustrating the treatment process using HA-aPS-aCPT NPs. The formation of HA-aPS-aCPT NPs was first achieved through the self-assembly of HA-CD, aCPT and aPS (A). After which, the therapeutic efficacy was tested on mouse models. Accumulation of HA-aPS-aCPT NPs was achieved after intravenous injection of NPs (B). Light with a suitable wavelength, *i.e.*, 660 nm was then irradiated. The combination PDT and chemotherapy were achieved after CD44 mediated endocytosis of HA-aPS-aCPT NPs coupled with light irradiation in five steps (C).

In light of the need for activation of prodrug using red or NIR light, various activatable systems relying on inorganic materials[31] such as upconversion crystals[19] and gold NPs[46,47] was developed. However, the metabolism, biodistribution and blood circulation of inorganic nanosystem still require deeper investigations.[48] The biocompatibility, biosafety, and biodegradability are also important aspects toward clinical applications. On the other hand, organic materials that are biodegradable with high biocompatibility should be harnessed. Hyaluronic acid (HA), a natural occurring polysaccharide, is a promising candidate for biomedical applications.[49-52] Advantages of HA as a polymeric carrier include its high biocompatibility and low cytotoxicity as well as easy conjugation with small molecules *via* its carboxylic group.[53] HA has also been identified as a targeting ligand to the cluster determinant 44 (CD44) that is overly expressed on various tumor cells.[54-57] On account of over expression of the CD44 receptor on tumor cells as compared to normal cells, NPs modified with HA would attain preferential uptake into cancer tissues *via* the receptor-mediated endocytosis.[46,50,52,56-58]

Having these considerations, we herein design a NP system through supramolecular means using a hydrophilic polymer encapsulated with hydrophobic prodrug and photosensitizer in a controllable ratio to realize PDT and controlled release of chemotherapeutic drugs (Scheme 1). In this system, HA is conjugated with β-cyclodextrin (CD) to give HA-CD, in which CD could form the inclusion complex with adamantane conjugated photosensitizer and prodrug for effective encapsulation and formation of NPs. The inclusion complex formed by CD and adamantane provides the polymer with the amphiphilicity, enabling the self-assembly into NPs.[10,58-60] The two therapeutic components encapsulated include adamantane conjugated CPT (aCPT) as the prodrug *via* ROS-responsive thioketal bond and adamantane-conjugated 5,10,15,20-tetrakis(4-hydroxyphenyl)-21H,23H-porphine (aPS) as the photosensitizer. The

supramolecular assembly of the three components (*i.e.*, HA-CD, aCPT and aPS) gives HA-aPS-aCPT NPs as shown in Scheme 1. To fulfil the combination therapy, the NPs synthesized should first be internalized *via* the enhanced permeability and retention (EPR) effect and CD44 mediated endocytosis.[61,62] Following which, the irradiation of NPs with light leads to the generation of $^1O_2$ for PDT. The produced $^1O_2$ could also react with the thioketal linker on the aCPT prodrug to result in a cascaded release of free CPT. The advantages of this system are (1) passive targeting due to its nanoscale size and active targeting by HA *via* overly expressed CD44 receptor on cancer cells, (2) light activatable on-demand release of active drugs from prodrugs for spatiotemporal chemotherapy combined with PDT, (3) easy purifications of individual molecules (aCPT and aPS) as opposed to some amphiphilic prodrugs, and (4) high tunability in controllable dosage and ratio of photosensitizer and prodrug for personalized cancer treatment. Thus, this superior NP system presented selective and higher killing efficacy of cancer cells *via* combined PDT and chemotherapy after systemic administration, reducing side effects of conventional chemotherapeutics.

Results and Discussions

Synthesis. The synthetic procedures of HA-CD, aCPT and aPS are illustrated in Schemes S1-S3. The successful synthesis of aCPT and aPS was confirmed by ^{1}H NMR spectra and electrospray ionization mass spectrometry (Figures S5 and S7). The HA-CD polymer was characterized by ^{1}H NMR spectrum (Figure S9). The conjugation degree of CD was determined to be 6.56%, which is equivalent to 15.2 HA monomer per 1 CD. This observation indicates that HA-CD is ideal for targeting purpose, as several reports showed that at least six consecutive HA sugar monomers are required for targeting CD44 receptor.[63,64]

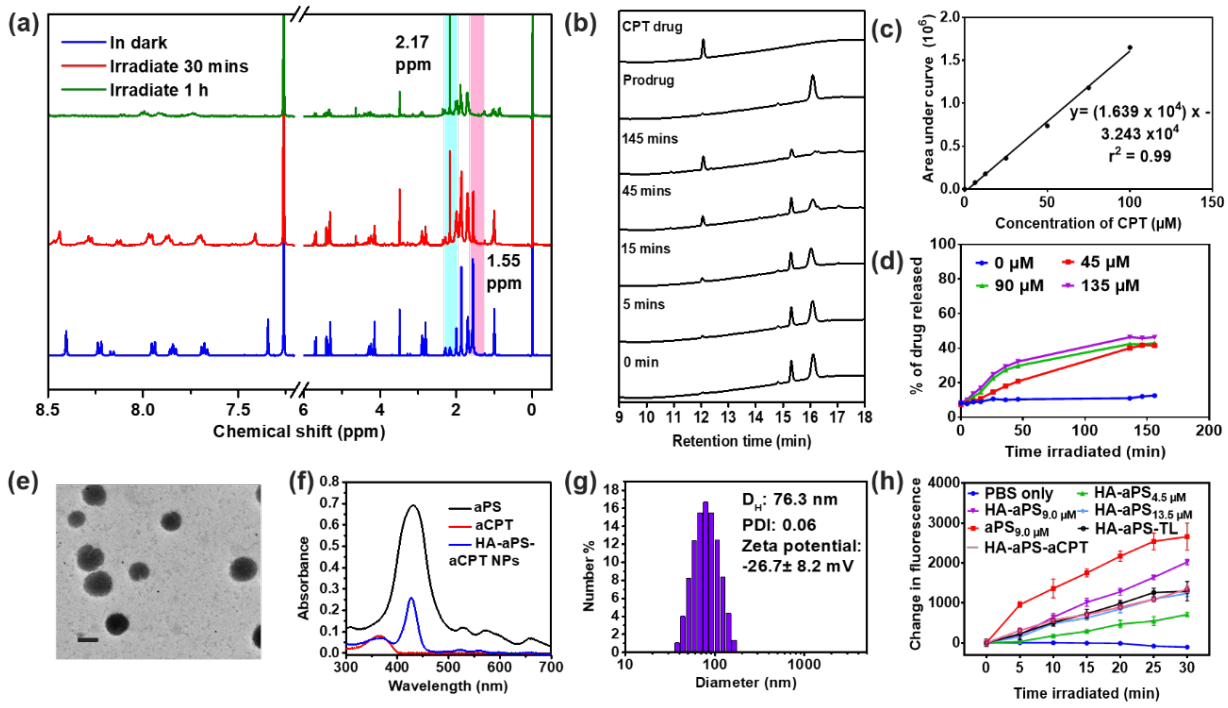

Figure 1. Characterizations of aPS, aCPT and HA-aPS-aCPT NPs. (a) ^{1}H NMR analysis for the cleavage of thioketal linker after irradiation for 30 min and 1 h. (b) HPLC analysis for CPT release from aCPT (retention time of CPT, aPS and aCPT were 12.0, 15.3 and 16.1 min respectively). (c) Calibration curve of CPT obtained from corresponding HPLC curve. (d) Drug release profile determined by HPLC when 45 μM aCPT was co-incubated with aPS with concentrations of 45, 90 and 135 μM. (e) TEM image of HA-aPS-aCPT NPs. Scale bar: 100 nm. (f) UV-vis absorption of aPS, aCPT and HA-aPS-aCPT NPs. (g) Hydrodynamic diameter of HA-aPS-aCPT NPs using DLS. (h) SOSG results obtained for different samples (HA-aPS at different concentrations of 4.5, 9.0 and 13.5 μM; aPS, HA-aPS-TL and HA-aPS-aCPT NPs with an equivalent aPS concentration of 9.0 μM) after irradiation of light at different time intervals measured at 530 nm when excited at 494 nm.

Cleavage of Thioketal Linker from aCPT. The cleavage of the thioketal linker on aCPT was investigated using ^{1}H NMR spectra and high performance liquid chromatography (HPLC). When $^1O_2$ reacts with the thioketal linker, the intermediate product could undergo nucleophilic attacking and release acetone as one of the by-products (Scheme 1). Upon irradiation of the mixture of aPS and aCPT with light, the formation of acetone was indicated by the presence of the resonance at 2.17 ppm in the NMR spectrum as shown in Figure 1a. Under longer irradiation time, the integral of this resonance increased. Concurrently, the integral of the resonance at 1.55 ppm assigned to the methyl group on the thioketal unit decreased, indicating that the degradation of the thioketal linker by the generated $^1O_2$ occurred. To further confirm that free CPT could be released under light irradiation, the HPLC study of the reaction was performed (Figure 1b). The amount of CPT was quantified by external standard calibration method as presented in Figure 1c, showing linear dependence of the area with respect to the concentration of CPT. Under longer irradiation time, the released amount of CPT increased as indicated by greater area at the retention time of 12.0 min. This result shows that the amount of free CPT released was dependent on the irradiation time as shown in Figure 1d. When the photosensitizer with higher concentrations was co-doped in the mixture, the amount of free CPT released under the same irradiation time and light power density was higher, revealing that the release of free CPT was also dependent on the amount of photosensitizer. A gradual decrease in the peak intensity of aPS upon the light irradiation indicates possible photobleaching of aPS by the produced $^1O_2$. The generated CPT was further proven using high-resolution mass spectrometry (HRMS) as shown in Figure S10 (calculated $[M+H^+]$ = 349.1188 m/z, found = 349.1189). These results indicated that the synthesized prodrug was indeed capable of releasing free CPT in ROS-responsive release manner.

Photophysical Properties of aPS and ROS Detection. The photophysical properties of aPS were investigated through UV-vis-NIR spectroscopy as shown in Figure 1f. Porphyrins are known to contain a Soret band and four Q bands in their absorbance.[65] In the case of aPS, the absorbance maximum obtained at 431 nm was assigned as the Soret band, and four Q bands at 530, 572, 603 and 657 nm were also observed. These observations indicate that the photophysical properties of the porphyrin unit are well preserved after the adamantane functionalization. To investigate the ROS generation ability of aPS, singlet oxygen sensor green (SOSG) was utilized for capturing the $^1O_2$ generated upon irradiation of light on aPS, where the amount of $^1O_2$ produced was correlated to the increase in SOSG fluorescence. HA-aPS samples with three concentrations ([aPS] = 4.5, 9.0, and 13.5 μM) were examined for the singlet oxygen generation. HA-aPS with [aPS] = 9.0 μM showed the highest increase in fluorescence as compared to the other two samples (Figure 1h). This could be because, at lower concentration of aPS (4.5 μM), the singlet oxygen generated was limited, while at higher concentration (13.5 μM), the quenching of the photosensitizer led to a decrease in the $^1O_2$ generation. Thus, the amount of aPS chosen in the final NPs was 9.0 μM. After which, $^1O_2$ generated by free aPS, HA-aPS-TL, and HA-aPS-aCPT ([aPS] = 9.0 μM) was investigated in aqueous solution. TL is a control linker with the thioketal bond but has no CPT drug attached. The amount of $^1O_2$ generated follows this sequence: free aPS > HA-aPS > HA-aPS-TL ≈ HA-aPS-aCPT. HA-aPS had lower $^1O_2$ generation yield than free aPS, because aPS was encapsulated within the HA-aPS NPs having possible aggregation effect.[66] Comparing HA-aPS, HA-aPS-TL and HA-aPS-aCPT, HA-aPS-TL and HA-aPS-aCPT had lower $^1O_2$ yield than HA-aPS, because some of the $^1O_2$ generated was utilized for the cleavage of thioketal linker. Since the same molar ratio of TL linker and aCPT ([TL] = [aCPT]) was added in HA-aPS-TL and HA-aPS-aCPT, they gave

similar $^1O_2$ yield. Despite some of the $^1O_2$ was used for the cleavage of thioketal bond, the generated $^1O_2$ was still high enough for possible PDT of cancer, fulfilling the dual therapeutic treatment.

Self-Assembly Characterization. Employment of β-CD and adamantane was based on their high association constant of approximately 1×10^5 mol/L in water.[67,68] Thus, it was hypothesized that the adamantane unit of aPS and aCPT would form the inclusion complex with β-CD of HA-CD to give an ampliphilic polymer. The self-assembly of this ampliphilic polymer gives HA-aPS-aCPT NPs with hydrophobic core (aPS and aCPT) and hydrophilic shell (HA). The association constants of aPS and aCPT with β-CD as the reference host were calculated from Hildebrand-Benesi plot.[69] aPS and aCPT with β-CD were found to have the association constants of 3.58×10^3 L/mol and 2.55×10^3 L/mol respectively (Figure S11), indicating their good binding capability. After which, the critical aggregation concentration (CAC) of HA-aPS-aCPT was determined by the pyrene probe (Table S1).[10,70] The CAC value was lower as the amount of the hydrophobic component increased, indicating strong hydrophobic interaction within the hydrophobic core (Figure S12).[58,60,71] When increasing the amount of hydrophobic adamantane moiety, the NP size measured by dynamic light scattering (DLS) decreased on account of having more compact hydrophobic core,[58,72] giving better size distribution as shown by lower polydispersion index (PDI).

Characterization of NPs. The HA-aPS-aCPT NPs with hydrophobic core (aPS and aCPT) and hydrophilic shell (HA) were formed by the supramolecular assembly of hydrophilic HA-CD and hydrophobic aPS and aCPT. One of the advantages of such supramolecular system is that the amount of photosensitizers and drugs could be facilely adjusted. Six NPs with different photosensitizer to prodrug ratios (1:0, 3:1, 2:1, 1:2, 1:3 and 0:1) were mainly fabricated. The

morphologies of the NPs were found to be spherical as visualized by transmission electron microscopy (TEM) (Figure S13). The measurement of their hydrodynamic diameters using DLS gave 76.3 to 302.4 nm (Figure S14). The absorption spectra of the six NPs with different amounts of aCPT and aPS show quantitative loading efficiency since the absorbances of aPS and aCPT did not decrease after the dialysis. Hypsochromic shifts were observed for the NPs with increasing amounts of photosensitizers due to the aggregation effect of the photosensitizers within the NPs (Figure S15). Finally, HA-aPS-aCPT NPs with photosensitizer to prodrug ratio of 2:1 ([HA] = 1 mg/mL, [aPS] = 9.0 μM, and [aCPT]= 4.5 μM) were chosen for further cell studies and *in vivo* applications. A concentration of 9.0 μM was determined to present the highest $^1O_2$ production from the SOSG experiment. With greater proportion of photosensitizers, a portion of the photosensitizers can be used to fulfill on-demand release of chemotherapeutic drugs by the cleavage of ROS-responsive bond, and the other portion can be employed for the PDT purpose. In this specific case, the drug loading capacity for aCPT and aPS was determined to be 3.24% and 7.55%, respectively. The morphology of HA-aPS-aCPT NPs visualized by TEM (Figure 1e) showed monodispersed spherical NPs. DLS measurements gave hydrodynamic size of 76.3 nm and zeta potential of -26.7± 8.2 mV as shown in Figure 1g. The NPs with the suitable size indicate their promising tumor accumulation through the EPR effect. The negatively charged zeta potential suggests that the HA unit is on the surface of the NPs, similar to typical HA systems reported.[52,73,74] The CAC was determined to be 0.05 mg/mL of the polymer, meaning that the NPs were stable even at low concentrations of the polymer. The chosen HA-aPS-aCPT NPs showed characteristic absorbance peaks of aCPT at 361 nm and aPS at 427, 524, 560 and 598 nm (Figure 1f), indicating successful encapsulation of both components.

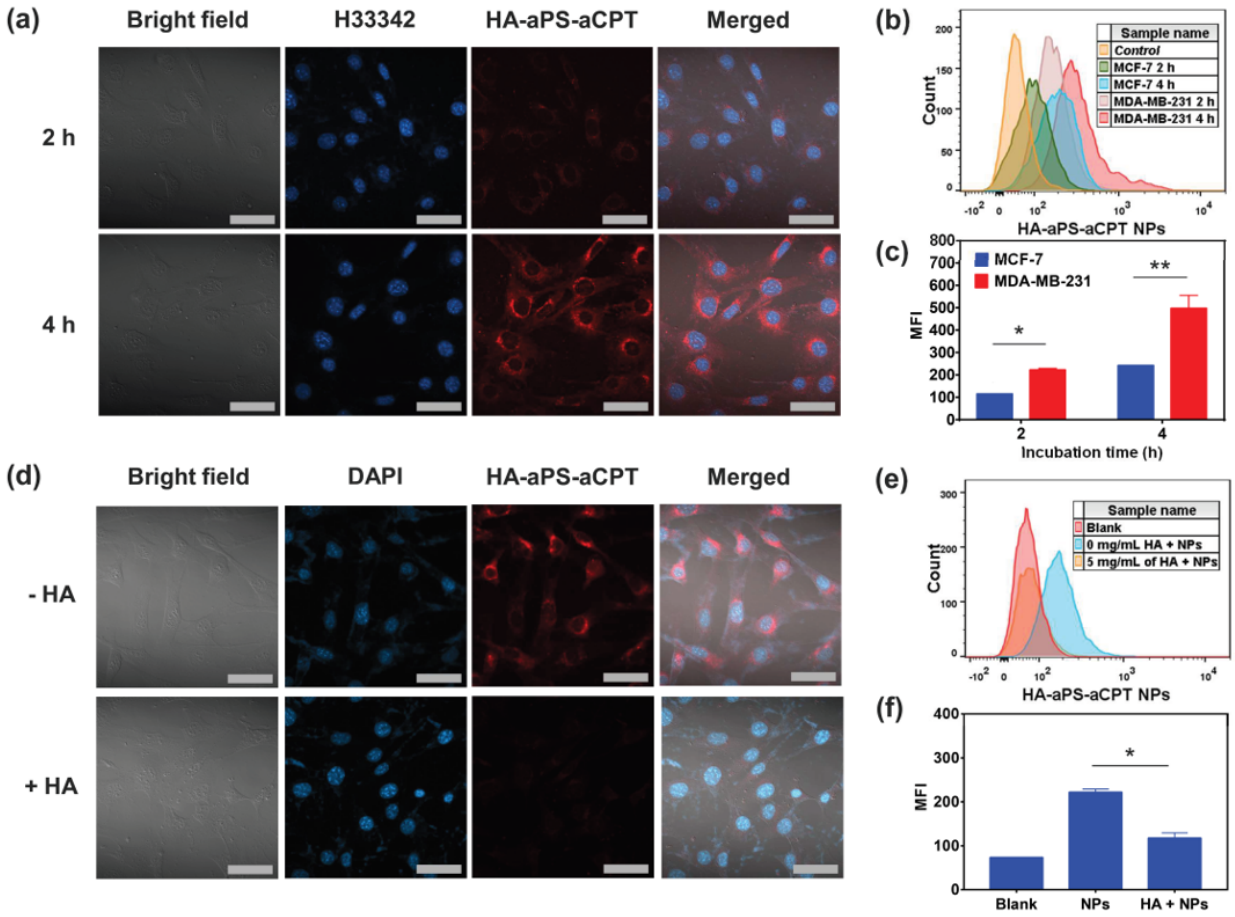

Figure 2. *In vitro* studies on cellular uptake and CD44 targeting. (a) Fluorescence images of MDA-MB-231 (CD44+ cells) when incubated with HA-aPS-aCPT NPs (100 μg/mL) for different incubation times (2 h and 4 h). (b) Representative plots of cell populations determined by flow cytometric analysis for MDA-MB-231 (CD44+ cells) and MCF-7 (CD44- cells) internalized by HA-aPS-aCPT NPs at different incubation times (2 h and 4 h). (c) Mean fluorescence intensity of HA-aPS-aCPT NPs in different cells at different incubation times. (d) Fluorescence images of MDA-MB-231 (CD44+ cells) incubated with HA-aPS-aCPT NPs (100 μg/mL) for 2 h when pretreated without and with free HA (5 mg/mL). (e) Representative plots and (f) mean fluorescence intensity of cell populations determined by flow cytometric analysis

for cellular uptake of HA-aPS-aCPT NPs pretreated without and with free HA. Scale bar: 50 μm. P values were calculated using student's t-test. * represents $p < 0.05$, ** represents $p < 0.001$.

Cellular Uptake and *In Vitro* Targeting Ability. MDA-MB-231 breast cancer cells were chosen as the cell line because their overly expressed CD44 could be targeted by HA.[49] The accumulation of HA-aPS-aCPT NPs in cells was visualized using confocal laser scanning microscope (CLSM) and measured using flow cytometry. Confocal images showed time-dependent uptake, *i.e.*, greater fluorescence with longer incubation time (Figure 2a). To determine the capability of the HA-aPS-aCPT NPs for targeting CD44 receptors, MDA-MB-231 (CD44-rich: $CD44^+$) and MCF-7 (CD44-poor: $CD44^-$) cells were selected for cellular comparative studies. Using flow cytometry analysis (Figure 2b,c) after the incubation of HA-aPS-aCPT NPs at 2 h and 4 h, the mean fluorescence intensity (MFI) of MDA-MB-231 cells was 1.93-folds and 2.05-folds higher than that of MCF-7 cells respectively, indicating higher uptake of HA-aPS-aCPT NPs by MDA-MB-231 cells possibly due to the rich presence of CD44 receptors for efficient receptor-mediated cellular uptake. In addition, competitive inhibition study was carried out to confirm the cellular uptake of HA-aPS-aCPT NPs *via* CD44-mediated endocytosis using confocal imaging (Figure 2d) and flow cytometric analysis. The MDA-MB-231 cells pretreated with excess serum-free HA polymer showed 1.90-folds lower uptake of HA-aPS-aCPT NPs than untreated ones (Figure 2e,f). This observation suggested that both free HA and HA-aPS-aCPT NPs could competitively bind to CD44 receptors, confirming that the internalization pathway of HA-aPS-aCPT NPs was through CD44 receptor-mediated endocytosis.

***In Vitro* ROS Detection.** After confirming the internalization pathway of the NPs, we evaluated whether ROS could be produced *in vitro* when HA-aPS-aCPT NPs were illuminated with light. The intracellular ROS production induced by HA-aPS-aCPT NPs was determined in MDA-MB-231 cells using a general oxidative stress indicator, carboxy-DCFDA (Figure 3a). The fluorescence intensity of cells incubated with NPs and irradiated with light was the highest amongst other control groups, indicating the successful production of ROS by HA-aPS-aCPT NPs *in vitro*. The produced ROS from HA-aPS-aCPT NPs could be used not only for PDT, but also for the cleavage of the thioketal linker toward the drug release as previously discussed. The cleavage of the prodrug into its active form allows chemotherapy to be combined with PDT.

Cell Viability and Apoptosis Study. The cytotoxicity of the NPs was evaluated using MTT assays (Figure 3c). At the same equivalent molar concentrations, aCPT was found to be less toxic than free CPT due to the functionalization of the hydroxy group on the lactone ring that is important in the topoisomerase inhibition to result in the apoptosis in cells.[75,76] At high concentrations of NPs ([NPs] = 200 μg/mL), HA-aPS-aCPT displayed low cellular toxicity in the dark, showing high cell viability of 74.4%. Comparing HA-aPS-TL and HA-aPS-aCPT NPs under light irradiation, at low concentrations of 0 to 100 μg/mL, HA-aPS-aCPT NPs displayed higher cytotoxicity because the contained aCPT could be released as free CPT upon light irradiation, leading to combination PDT and chemotherapy. At the concentration of 200 μg/mL, however, HA-aPS-aCPT and HA-aPS-TL NPs showed similar high cytotoxicity possibly because PDT predominated. Flow cytometric analysis was used to quantify the amount of apoptotic MDA-MB-231 cells when treated with HA-aPS-aCPT NPs (Figure S16). When healthy MDA-MB-231 cells were treated with HA-aPS-TL and HA-aPS-aCPT NPs in the dark, the total amounts of apoptotic cells were low at 3.0% and 4.9%, respectively (Figure 3d). The numbers of

apoptotic cells for both HA-aPS-TL and HA-aPS-aCPT NPs under light irradiation were significantly higher than that in the dark. These results indicated that the NPs displayed minimal dark cytotoxicity and light irradiation was essential to induce their cellular toxicity.

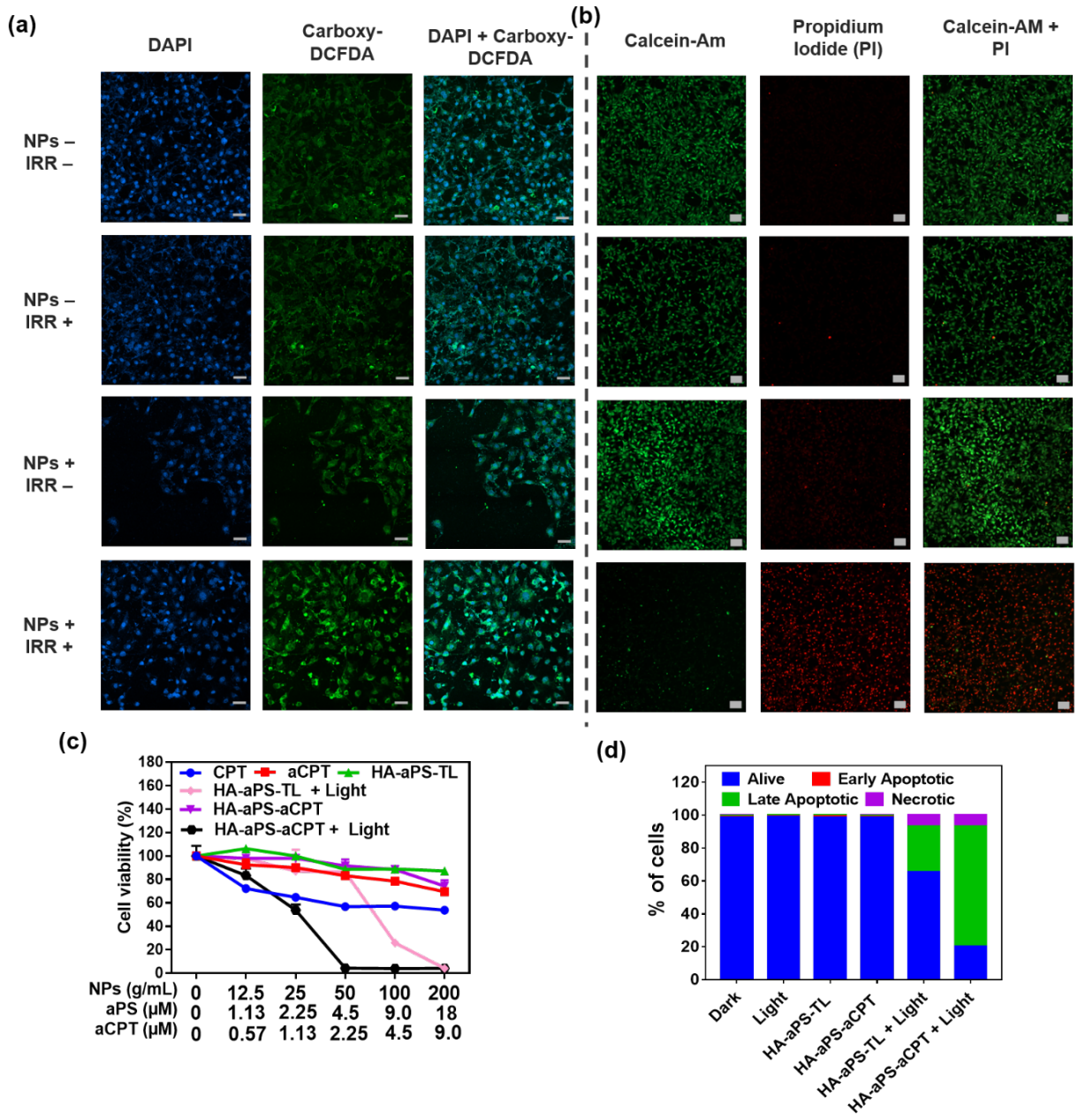

Figure 3. *In vitro* cytotoxicity studies on MDA-MD-231 cells. (a) Detection of ROS using carboxy-DCFDA (green). Nuclei were stained with 4',6-diamidino-2-phenylindole (DAPI, blue). Scale bar: 50 μm. (b) Live/dead assay on MDA-MB-231 (CD44+ cells) with and without NPs as

well as with and without light irradiation (IRR), where + means related treatment was done, and - means no such treatment was done. Scale bar: 100 μm. (c) Cell viability of MDA-MB-231 cells when incubated with free CPT, aCPT, HA-aPS-TL with and without light irradiation, and HA-aPS-aCPT with and without light irradiation at different concentrations. (d) Quantitative numbers of different cells obtained from apoptotic study using Annexin V FITC and PI.

According to the cellular apoptosis results, there was higher percentage of apoptotic cells incubated with HA-aPS-aCPT (72.8%) as compared to that of HA-aPS-TL NPs (27.8%), validating that CPT was released upon light irradiation to result in higher cellular toxicity. Live/dead confocal images of the cells irradiated with HA-aPS-aCPT NPs under light irradiation also showed higher number of red cells (propidium iodide (PI) stained cells) indicative of higher cellular toxicity (Figure 3b).

***In Vivo* Biodistribution.** Encouraged by the *in vitro* therapeutic results, the biodistribution and treatment efficiency of unmodified photosensitizer 5,10,15,20-tetrakis(4-hydroxyphenyl)-21H,23H-porphine (THPP) as well as HA-aPS-aCPT NPs were assessed *in vivo* using xenografted nude mouse models with triple negative breast cancer cells MDA-MB-231. THPP was used as a control for free photosensitizer without the nanocarrier. After THPP and HA-aPS-aCPT NPs were intravenously injected into the nude mice bearing MDA-MB-231 tumors, they were visualized (Figure 4a) using the *in vivo* imaging system (IVIS) at the wavelength of photosensitizers under different time intervals. Their accumulation in tumors was initially studied. A progressive accumulation of HA-aPS-aCPT NPs in the tumor was observed over time. On the other hand, no obvious accumulation of THPP in the tumor was observed at the end of 24 h. After 24 h, the mice were sacrificed, and major organs and tumors were harvested and

visualized. The HA-aPS-aCPT NPs were observed to accumulate in tumor, liver and spleen (Figure 4b). THPP was not found in the tumor, and it accumulated mainly in liver and spleen for the excretion.[77] Although HA-aPS-aCPT NPs have the ability to target tumors, they also showed the accumulation in liver and spleen for being excreted.

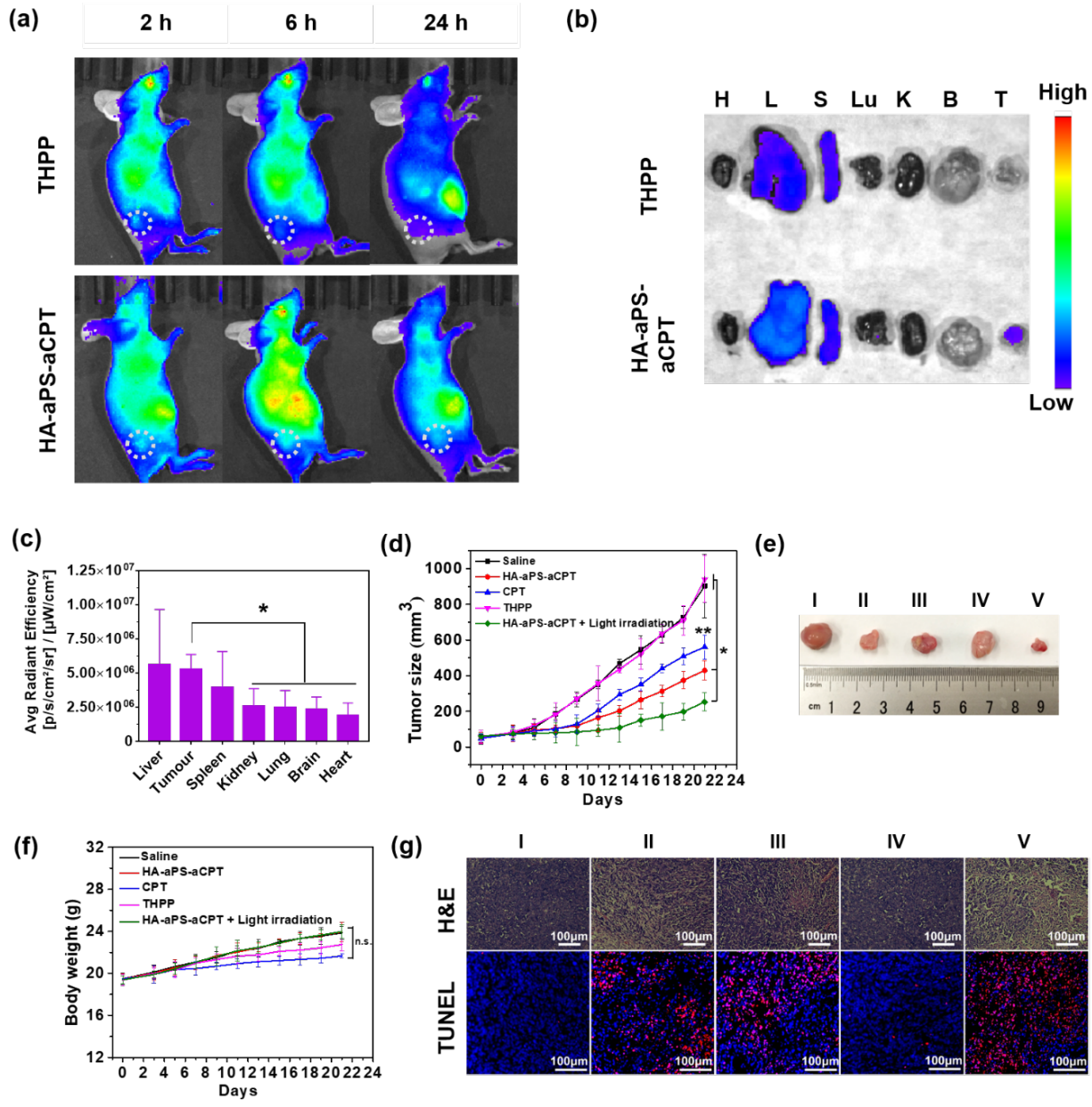

Figure 4. *In vivo* antitumor effect. (a) Biodistribution of THPP and HA-aPS-aCPT NPs at different time intervals after intravenous injection into mice. The tumors were indicated using

white circles. (b) *Ex vivo* fluorescence image of major organs and tumors excised from mice injected with THPP and HA-aPS-aCPT NPs. H, L, S, Lu, K, B and T stands for heart, liver, spleen, lung, kidney, brain and tumor, respectively. (c) Biodistribution of HA-aPS-aCPT NPs in various organs determined from (b). (d) Time-dependent tumor growth on mice with different treatments over a period of 21 days. (e) One of the excised tumors from each group at the end of day 21 from euthanized mice. (f) Body weights of mice with different treatments monitored over a period of 21 days. (g) H&E staining and TUNEL assay of tumor tissues from euthanized mice with different treatments. I: saline; II: HA-aPS-aCPT; III: CPT; IV: THPP; V: HA-aPS-aCPT + Light irradiation. P values were calculated using student's t-test. * represents $p < 0.05$, ** represents $p < 0.001$.

***In Vivo* Antitumor Efficacy.** The antitumor efficacy of the NPs was examined by using nude mice bearing MDA-MB-231 tumors. Five groups of mice were monitored over a period of 21 days after treated with different conditions (I: saline; II: HA-aPS-aCPT NPs; III: CPT; IV: THPP; V: HA-aPS-aCPT + Light irradiation). THPP is the free photosensitizer that was not modified by adamantane. As shown in Figure 4d,e, HA-aPS-aCPT NPs with light irradiation were able to largely suppress tumor growth as compared to the saline and THPP groups. The mean tumor volume (253.09 ± 50.27 mm^3) resulted from HA-aPS-aCPT NPs with light irradiation was significantly smaller than the saline (902.35 ± 178.48 mm^3) and THPP (939.98 ± 131.02 mm^3) groups. As discussed previously, the THPP photosensitizer did not accumulate in the tumor site (Figure 4a,b), explaining its minimal tumor inhibition effect. Although the administration of free CPT also delayed the growth of tumor (561.08 ± 67.43 mm^3), it exhibited obvious systemic toxicity as indicated by the lowest average body weight (Figure 4f). HA-aPS-aCPT NPs in the

dark also exhibited certain toxicity as shown by smaller mean tumor size (429.68 ± 54.01 mm^3). This observation could be explained by its better passive accumulation in tumor cells as well as high amount ROS already in tumor cells for releasing free CPT from aCPT.

In addition to the significant inhibition of tumor growth, HA-aPS-aCPT NPs accumulated mostly at tumor sites did not cause as much systemic toxicity as free CPT, indicated by the increased body weight of mice and Hematoxylin and Eosin (H&E) staining from various major mouse organs treated with HA-aPS-aCPT NPs (Figure 4f). H&E staining of tumors was conducted on all five groups of mice. Some minor damages in the tumor tissues when treated with HA-aPS-aCPT NPs and free CPT were observed, while serious damage was observed when mice were treated with HA-aPS-aCPT NPs under light irradiation (Figure 4g). This difference indicated that there was an enhancement of PDT with cascaded chemotherapy as compared to free CPT. Similar conclusion was drawn from terminal deoxynucleotidyl transferase dUTP nick end labeling (TUNEL) assay that detected apoptotic cells. After the treatments, the amount of TUNEL-positive cells was found to be in this order: V > II > III > IV > I. More red fluorescence from Cyanine 3 observed for tumor tissues of mice treated with HA-aPS-aCPT NPs under light irradiation indicated the highest number of apoptotic cells in these groups. After the treatment with HA-aPS-aCPT NPs, the H&E staining on major organs (heart, liver, spleen, lung and kidney) in different mice showed no obvious systematic toxicity (Figure S17). All these results demonstrated the feasibility of HA-aPS-aCPT NPs for combination PDT and chemotherapy, showing its high potency as a therapeutic protocol for the tumor treatment. Light irradiation alone did not inhibit the tumor growth or display any toxicity as indicated by the similar trend of tumor growth and minimal body weight change between saline and light irradiation treatment groups (Figure S18).

Conclusion

In conclusion, HA-aPS-aCPT NPs have been fabricated using three components (HA-CD, aPS and aCPT) *via* simple supramolecular means. The obtained NPs were monodispersed with almost 100% loading efficiency. The thioketal linker conjugated between adamantane and CPT in aCPT could be cleaved in a controlled manner when singlet oxygen is produced from aPS photosensitizer. The as-synthesized aPS photosensitizer was able to produce singlet oxygen upon the irradiation of 660 nm light. Targeting capability of HA was demonstrated at cellular level using competitive HA assays. High cellular toxicity was demonstrated when cancer cells were incubated with HA-aPS-aCPT NPs under light irradiation. Excellent tumor accumulation of HA-aPS-aCPT NPs in xenograft mouse models bearing MDA-MB-231 cancer was clearly due to passive targeting and CD44 receptor-mediated endocytosis. HA-aPS-aCPT NPs were able to significantly inhibit the tumor growth as compared with other control groups. Importantly, the present system capable of conducting combination chemotherapy and PDT displayed no obvious systemic toxicity, enabling its useful applications toward practical cancer treatment. The pharmacokinetics and pharmacodynamics of the current system would be investigated in our future research.

ASSOCIATED CONTENT

Supporting Information.

The Supporting Information is available free of charge on the ACS Publications website at DOI:

Scheme and synthesis procedures of HA-CD, aCPT and aPS; ^{1}H NMR spectrum of HA-CD; ^{1}H NMR and ESI-MS spectra of aCPT and aPS; Hildebrand-Benesi plots for aPS and aCPT; CAC, hydrodynamic size, PDI, TEM, DLS and absorbance of NPs; apoptosis study; H&E staining of major organs (PDF).

AUTHOR INFORMATION

Corresponding Author

* Zhong Luo: luozhong918@cqu.edu.cn

* Yanli Zhao: zhaoyanli@ntu.edu.sg

# The authors contributed equally to this work.

ACKNOWLEDGMENT

This research is supported by the Singapore Academic Research Fund (No. RG5/16, RG11/17 and RG114/17), the Singapore Agency for Science, Technology and Research (A*STAR) AME IRG grant (No. A1883c0005), and the Singapore National Research Foundation Investigatorship (No. NRF-NRFI2018-03).

REFERENCES

1. Singh, Y.; Palombo, M.; Sinko, P. J. Recent Trends in Targeted Anticancer Prodrug and Conjugate Design. *Curr. Med. Chem.* **2008,** *15*, 1802-1826.

2. Luo, C.; Sun, J.; Sun, B.; He, Z. Prodrug-Based Nanoparticulate Drug Delivery Strategies for Cancer Therapy. *Trends Pharmacol. Sci.* **2014,** *35*, 556-566.

3. Chen, H.; Jia, H.; Tham, H. P.; Qu, Q.; Xing, P.; Zhao, J.; Phua, S. Z. F.; Chen, G.; Zhao, Y. Theranostic Prodrug Vesicles for Imaging Guided Codelivery of Camptothecin and siRNA in Synergetic Cancer Therapy. *ACS Appl. Mater. Interfaces* **2017,** *9*, 23536-23543.

4. Mo, R.; Gu, Z. Tumor Microenvironment and Intracellular Signal-Activated Nanomaterials for Anticancer Drug Delivery. *Mater. Today* **2016,** *19*, 274-283.

5. Sun, W.; Jiang, T.; Lu, Y.; Reiff, M.; Mo, R.; Gu, Z. Cocoon-Like Self-Degradable DNA Nanoclew for Anticancer Drug Delivery. *J. Am. Chem. Soc.* **2014,** *136*, 14722-14725.

6. Yang, G.; Xu, L.; Chao, Y.; Xu, J.; Sun, X.; Wu, Y.; Peng, R.; Liu, Z. Hollow MnO_2 as a Tumor-Microenvironment-Responsive Biodegradable Nano-Platform for Combination Therapy Favoring Antitumor Immune Responses. *Nat. Commun.* **2017,** *8*, 902.

7. Zhang, Y.; Teh, C.; Li, M.; Ang, C. Y.; Tan, S. Y.; Qu, Q.; Korzh, V.; Zhao, Y. Acid-Responsive Polymeric Doxorubicin Prodrug Nanoparticles Encapsulating a Near-Infrared Dye for Combined Photothermal-Chemotherapy. *Chem. Mater.* **2016,** *28*, 7039-7050.

8. Wang, X.; Cai, X.; Hu, J.; Shao, N.; Wang, F.; Zhang, Q.; Xiao, J.; Cheng, Y. Glutathione-Triggered "Off–On" Release of Anticancer Drugs from Dendrimer-Encapsulated Gold Nanoparticles. *J. Am. Chem. Soc.* **2013,** *135*, 9805-9810.

9. Xiang, H.; Chen, H.; Tham, H. P.; Phua, S. Z. F.; Liu, J.-G.; Zhao, Y. Cyclometalated Iridium(III)-Complex-Based Micelles for Glutathione-Responsive Targeted Chemotherapy and Photodynamic Therapy. *ACS Appl. Mater. Interfaces* **2017,** *9*, 27553-27562.

10. Zhang, Y.; Yang, D.; Chen, H.; Lim, W. Q.; Phua, F. S. Z.; An, G.; Yang, P.; Zhao, Y. Reduction-Sensitive Fluorescence Enhanced Polymeric Prodrug Nanoparticles for Combinational Photothermal-Chemotherapy. *Biomaterials* **2018,** *163*, 14-24.

11. Zhang, H.; Fei, J.; Yan, X.; Wang, A.; Li, J. Enzyme-Responsive Release of Doxorubicin from Monodisperse Dipeptide-Based Nanocarriers for Highly Efficient Cancer Treatment *in Vitro*. *Adv. Funct. Mater.* **2015,** *25*, 1193-1204.

12. Ortiz de Montellano, P. R. Cytochrome P450-Activated Prodrugs. *Future Med. Chem.* **2013,** *5*, 213-228.

13. Feng, L.; Cheng, L.; Dong, Z.; Tao, D.; Barnhart, T. E.; Cai, W.; Chen, M.; Liu, Z. Theranostic Liposomes with Hypoxia-Activated Prodrug to Effectively Destruct Hypoxic Tumors Post-Photodynamic Therapy. *ACS Nano* **2017,** *11*, 927-937.

14. Qian, C.; Yu, J.; Chen, Y.; Hu, Q.; Xiao, X.; Sun, W.; Wang, C.; Feng, P.; Shen, Q.-D.; Gu, Z. Light-Activated Hypoxia-Responsive Nanocarriers for Enhanced Anticancer Therapy. *Adv. Mater.* **2016,** *28*, 3313-3320.

15. Shirakura, T.; Kelson, T. J.; Ray, A.; Malyarenko, A. E.; Kopelman, R. Hydrogel Nanoparticles with Thermally Controlled Drug Release. *ACS Macro Lett.* **2014,** *3*, 602-606.

16. Yang, G.; Liu, J.; Wu, Y.; Feng, L.; Liu, Z. Near-Infrared-Light Responsive Nanoscale Drug Delivery Systems for Cancer Treatment. *Coord. Chem. Rev.* **2016,** *320–321*, 100-117.

17. Liu, L.-H.; Qiu, W.-X.; Li, B.; Zhang, C.; Sun, L.-F.; Wan, S.-S.; Rong, L.; Zhang, X.-Z. A Red Light Activatable Multifunctional Prodrug for Image-Guided Photodynamic Therapy and Cascaded Chemotherapy. *Adv. Funct. Mater.* **2016,** *26*, 6257-6269.

18. Yue, C.; Yang, Y.; Zhang, C.; Alfranca, G.; Cheng, S.; Ma, L.; Liu, Y.; Zhi, X.; Ni, J.; Jiang, W.; Song, J.; de la Fuente, J. M.; Cui, D. ROS-Responsive Mitochondria-Targeting Blended Nanoparticles: Chemo- and Photodynamic Synergistic Therapy for Lung Cancer with On-Demand Drug Release upon Irradiation with a Single Light Source. *Theranostics* **2016,** *6*, 2352-2366.

19. Yue, C.; Zhang, C.; Alfranca, G.; Yang, Y.; Jiang, X.; Yang, Y.; Pan, F.; de la Fuente, J. M.; Cui, D. Near-Infrared Light Triggered ROS-activated Theranostic Platform based on Ce6-CPT-UCNPs for Simultaneous Fluorescence Imaging and Chemo-Photodynamic Combined Therapy. *Theranostics* **2016,** *6*, 456-469.

20. Chen, H.; Zhao, Y. Applications of Light-Responsive Systems for Cancer Theranostics. *ACS Appl. Mater. Interfaces* **2018,** *10*, 21021-21034.

21. Schroeder, A.; Honen, R.; Turjeman, K.; Gabizon, A.; Kost, J.; Barenholz, Y. Ultrasound Triggered Release of Cisplatin from Liposomes in Murine Tumors. *J. Controlled Release* **2009,** *137*, 63-68.

22. Couture, O.; Foley, J.; Kassell, N. F.; Larrat, B.; Aubry, J.-F. Review of Ultrasound Mediated Drug Delivery for Cancer Treatment: Updates from Pre-Clinical Studies. *Transl. Cancer Res.* **2014,** *3*, 494-511.

23. Ai, X.; Mu, J.; Xing, B. Recent Advances of Light-Mediated Theranostics. *Theranostics* **2016,** *6*, 2439-2457.

24. Jiang, M. Y.; Dolphin, D. Site-Specific Prodrug Release Using Visible Light. *J. Am. Chem. Soc.* **2008,** *130*, 4236-4237.

25. Fan, N.-C.; Cheng, F.-Y.; Ho, J.-a. A.; Yeh, C.-S. Photocontrolled Targeted Drug Delivery: Photocaged Biologically Active Folic Acid as a Light-Responsive Tumor-Targeting Molecule. *Angew. Chem. Int. Ed.* **2012,** *51*, 8806-8810.

26. Brown, P. K.; Qureshi, A. T.; Moll, A. N.; Hayes, D. J.; Monroe, W. T. Silver Nanoscale Antisense Drug Delivery System for Photoactivated Gene Silencing. *ACS Nano* **2013,** *7*, 2948-2959.

27. Hossion, A. M. L.; Bio, M.; Nkepang, G.; Awuah, S. G.; You, Y. Visible Light Controlled Release of Anticancer Drug through Double Activation of Prodrug. *ACS Med. Chem. Lett.* **2013,** *4*, 124-127.

28. Sheehan, J. C.; Umezawa, K. Phenacyl Photosensitive Blocking Groups. *J. Org. Chem.* **1973,** *38*, 3771-3774.

29. Shao, Q.; Jiang, T.; Ren, G.; Cheng, Z.; Xing, B. Photoactivable Bioluminescent Probes for Imaging Luciferase Activity. *Chem. Commun.* **2009,** 4028-4030.

30. Zhao, L.; Peng, J.; Huang, Q.; Li, C.; Chen, M.; Sun, Y.; Lin, Q.; Zhu, L.; Li, F. Near-Infrared Photoregulated Drug Release in Living Tumor Tissue via Yolk-Shell Upconversion Nanocages. *Adv. Funct. Mater.* **2014,** *24*, 363-371.

31. Kim, H.; Chung, K.; Lee, S.; Kim, D. H.; Lee, H. Near-Infrared Light-Responsive Nanomaterials for Cancer Theranostics. *Wiley Interdiscip. Rev. Nanomed. Nanobiotechnol.* **2016,** *8*, 23-45.

32. Li, Y.; Lv, S.; Song, Z.; Dang, J.; Li, X.; He, H.; Xu, X.; Zhou, Z.; Yin, L. Photodynamic Therapy-Mediated Remote Control of Chemotherapy toward Synergistic Anticancer Treatment. *Nanoscale* **2018,** *10*, 14554-14562.

33. He, H.; Zhu, R.; Sun, W.; Cai, K.; Chen, Y.; Yin, L. Selective Cancer Treatment *via* Photodynamic Sensitization of Hypoxia-Responsive Drug Delivery. *Nanoscale* **2018,** *10*, 2856-2865.

34. Gorka, A. P.; Nani, R. R.; Zhu, J.; Mackem, S.; Schnermann, M. J. A Near-IR Uncaging Strategy Based on Cyanine Photochemistry. *J. Am. Chem. Soc.* **2014,** *136*, 14153-14159.

35. Nani, R. R.; Gorka, A. P.; Nagaya, T.; Kobayashi, H.; Schnermann, M. J. Near-IR Light-Mediated Cleavage of Antibody–Drug Conjugates Using Cyanine Photocages. *Angew. Chem. Int. Ed.* **2015,** *54*, 13635-13638.

36. Nani, R. R.; Gorka, A. P.; Nagaya, T.; Yamamoto, T.; Ivanic, J.; Kobayashi, H.; Schnermann, M. J. *In Vivo* Activation of Duocarmycin–Antibody Conjugates by Near-Infrared Light. *ACS Cent. Sci.* **2017,** *3*, 329-337.

37. Rajaputra, P.; Bio, M.; Nkepang, G.; Thapa, P.; Woo, S.; You, Y. Anticancer Drug Released from Near IR-activated Prodrug Overcomes Spatiotemporal Limits of Singlet Oxygen. *Bioorg. Med. Chem.* **2016,** *24*, 1540-1549.

38. Wang, J.; Sun, X.; Mao, W.; Sun, W.; Tang, J.; Sui, M.; Shen, Y.; Gu, Z. Tumor Redox Heterogeneity-Responsive Prodrug Nanocapsules for Cancer Chemotherapy. *Adv. Mater.* **2013,** *25*, 3670-3676.

39. Luo, C.; Sun, J.; Liu, D.; Sun, B.; Miao, L.; Musetti, S.; Li, J.; Han, X.; Du, Y.; Li, L.; Huang, L.; He, Z. Self-Assembled Redox Dual-Responsive Prodrug-Nanosystem Formed by Single Thioether-Bridged Paclitaxel-Fatty Acid Conjugate for Cancer Chemotherapy. *Nano Lett.* **2016,** *16*, 5401-5408.

40. Deepagan, V. G.; Kwon, S.; You, D. G.; Nguyen, V. Q.; Um, W.; Ko, H.; Lee, H.; Jo, D.-G.; Kang, Y. M.; Park, J. H. *In Situ* Diselenide-Crosslinked Polymeric Micelles for ROS-Mediated Anticancer Drug Delivery. *Biomaterials* **2016,** *103*, 56-66.

41. Kim, E.-J.; Bhuniya, S.; Lee, H.; Kim, H. M.; Cheong, C.; Maiti, S.; Hong, K. S.; Kim, J. S. An Activatable Prodrug for the Treatment of Metastatic Tumors. *J. Am. Chem. Soc.* **2014,** *136*, 13888-13894.

42. Kwon, J.; Kim, J.; Park, S.; Khang, G.; Kang, P. M.; Lee, D. Inflammation-Responsive Antioxidant Nanoparticles Based on a Polymeric Prodrug of Vanillin. *Biomacromolecules* **2013,** *14*, 1618-1626.

43. Shim, M. S.; Xia, Y. A Reactive Oxygen Species (ROS)-Responsive Polymer for Safe, Efficient, and Targeted Gene Delivery in Cancer Cells. *Angew. Chem. Int. Ed.* **2013,** *52*, 6926-6929.

44. Xu, Q.; He, C.; Xiao, C.; Chen, X. Reactive Oxygen Species (ROS) Responsive Polymers for Biomedical Applications. *Macromol. Biosci.* **2016,** *16*, 635-646.

45. Pei, Q.; Hu, X.; Zheng, X.; Liu, S.; Li, Y.; Jing, X.; Xie, Z. Light-Activatable Red Blood Cell Membrane-Camouflaged Dimeric Prodrug Nanoparticles for Synergistic Photodynamic/Chemotherapy. *ACS Nano* **2018,** *12*, 1630-1641.

46. Tham, H. P.; Chen, H.; Tan, Y. H.; Qu, Q.; Sreejith, S.; Zhao, L.; Venkatraman, S. S.; Zhao, Y. Photosensitizer Anchored Gold Nanorods for Targeted Combinational Photothermal and Photodynamic Therapy. *Chem. Commun.* **2016,** *52*, 8854-8857.

47. Dreaden, E. C.; Mackey, M. A.; Huang, X.; Kang, B.; El-Sayed, M. A. Beating Cancer in Multiple Ways Using Nanogold. *Chem. Soc. Rev.* **2011,** *40*, 3391-3404.

48. Fadeel, B.; Garcia-Bennett, A. E. Better Safe than Sorry: Understanding the Toxicological Properties of Inorganic Nanoparticles Manufactured for Biomedical Applications. *Adv. Drug Delivery Rev.* **2010,** *62*, 362-374.

49. Mattheolabakis, G.; Milane, L.; Singh, A.; Amiji, M. M. Hyaluronic Acid Targeting of CD44 for Cancer Therapy: From Receptor Biology to Nanomedicine. *J. Drug Targeting* **2015,** *23*, 605-618.

50. Bae, K. H.; Tan, S.; Yamashita, A.; Ang, W. X.; Gao, S. J.; Wang, S.; Chung, J. E.; Kurisawa, M. Hyaluronic Acid-Green Tea Catechin Micellar Nanocomplexes: Fail-Safe Cisplatin Nanomedicine for the Treatment of Ovarian Cancer without Off-Target Toxicity. *Biomaterials* **2017,** *148*, 41-53.

51. Lin, W. J.; Lee, W. C.; Shieh, M. J. Hyaluronic Acid Conjugated Micelles Possessing CD44 Targeting Potential for Gene Delivery. *Carbohydr. Polym.* **2017,** *155*, 101-108.

52. Zhu, Q.; Chen, X.; Xu, X.; Zhang, Y.; Zhang, C.; Mo, R. Tumor-Specific Self-Degradable Nanogels as Potential Carriers for Systemic Delivery of Anticancer Proteins. *Adv. Funct. Mater.* **2018,** *28*, 1707371.

53. Kim, H.; Jeong, H.; Han, S.; Beack, S.; Hwang, B. W.; Shin, M.; Oh, S. S.; Hahn, S. K. Hyaluronate and Its Derivatives for Customized Biomedical Applications. *Biomaterials* **2017,** *123*, 155-171.

54. Mo, R.; Jiang, T.; DiSanto, R.; Tai, W.; Gu, Z. ATP-Triggered Anticancer Drug Delivery. *Nat. Commun.* **2014,** *5*, 3364.

55. Götte, M.; Yip, G. W. Heparanase, Hyaluronan, and CD44 in Cancers: A Breast Carcinoma Perspective. *Cancer Res.* **2006,** *66*, 10233-10237.

56. Naor, D.; Sionov, R. V.; Ish-Shalom, D. CD44: Structure, Function and Association with the Malignant Process. In *Advances in Cancer Research*, Woude, G. F. V.; Klein, G., Ed.; Academic Press: Cambridge, 1997; Vol. 71, pp 241-319.

57. Ponta, H.; Sherman, L.; Herrlich, P. A. CD44: From Adhesion Molecules to Signalling Regulators. *Nat. Rev. Mol. Cell Biol.* **2003,** *4*, 33-45.

58. Choi, K. Y.; Chung, H.; Min, K. H.; Yoon, H. Y.; Kim, K.; Park, J. H.; Kwon, I. C.; Jeong, S. Y. Self-Assembled Hyaluronic Acid Nanoparticles for Active Tumor Targeting. *Biomaterials* **2010,** *31*, 106-114.

59. Fan, H.; Hu, Q.-D.; Xu, F.-J.; Liang, W.-Q.; Tang, G.-P.; Yang, W.-T. *In Vivo* Treatment of Tumors Using Host-Guest Conjugated Nanoparticles Functionalized with Doxorubicin and Therapeutic Gene pTRAIL. *Biomaterials* **2012,** *33*, 1428-1436.

60. Hu, Q.; Li, W.; Hu, X.; Hu, Q.; Shen, J.; Jin, X.; Zhou, J.; Tang, G.; Chu, P. K. Synergistic Treatment of Ovarian Cancer by Co-Delivery of Survivin shRNA and Paclitaxel *via* Supramolecular Micellar Assembly. *Biomaterials* **2012,** *33*, 6580-6591.

61. Sun, T.; Zhang, Y. S.; Pang, B.; Hyun, D. C.; Yang, M.; Xia, Y. Engineered Nanoparticles for Drug Delivery in Cancer Therapy. *Angew. Chem. Int. Ed.* **2014,** *53*, 12320-12364.

62. Maeda, H., The Enhanced Permeability and Retention (EPR) Effect in Tumor Vasculature: The Key Role of Tumor-Selective Macromolecular Drug Targeting. *Adv. Enzyme Regul.* **2001,** *41*, 189-207.

63. Yang, Y.; Zhang, Y.-M.; Chen, Y.; Chen, J.-T.; Liu, Y. Polysaccharide-Based Noncovalent Assembly for Targeted Delivery of Taxol. *Sci. Rep.* **2016,** *6*, 19212.

64. Jaracz, S.; Chen, J.; Kuznetsova, L. V.; Ojima, I. Recent Advances in Tumor-Targeting Anticancer Drug Conjugates. *Bioorg. Med. Chem.* **2005,** *13*, 5043-5054.

65. Huang, X.; Nakanishi, K.; Berova, N. Porphyrins and Metalloporphyrins: Versatile Circular Dichroic Reporter Groups for Structural Studies. *Chirality* **2000,** *12*, 237-255.

66. Lambert, C. R.; Reddi, E.; Spikes, J. D.; Rodgers, M. A. J.; Jori, G. The Effects of Porphyrin Structure and Aggregation State on Photosensitized Processes in Aqueous and Micellar Media. *Photochem. Photobiol.* **1986,** *44*, 595-601.

67. Hu, Q.-D.; Tang, G.-P.; Chu, P. K. Cyclodextrin-Based Host–Guest Supramolecular Nanoparticles for Delivery: From Design to Applications. *Acc. Chem. Res.* **2014,** *47*, 2017-2025.

68. Chen, G.; Jiang, M. Cyclodextrin-Based Inclusion Complexation Bridging Supramolecular Chemistry and Macromolecular Self-Assembly. *Chem. Soc. Rev.* **2011,** *40*, 2254-2266.

69. Ang, C. Y.; Tan, S. Y.; Wang, X.; Zhang, Q.; Khan, M.; Bai, L.; Tamil Selvan, S.; Ma, X.; Zhu, L.; Nguyen, K. T.; Tan, N. S.; Zhao, Y. Supramolecular Nanoparticle Carriers Self-Assembled from Cyclodextrin- and Adamantane-Functionalized Polyacrylates for Tumor-Targeted Drug Delivery. *J. Mater. Chem. B* **2014,** *2*, 1879-1890.

70. Aguiar, J.; Carpena, P.; Molina-Bolívar, J. A.; Carnero Ruiz, C. On the Determination of the Critical Micelle Concentration by the Pyrene 1:3 Ratio Method. *J. Colloid Interface Sci.* **2003,** *258*, 116-122.

71. Owen, S. C.; Chan, D. P. Y.; Shoichet, M. S. Polymeric Micelle Stability. *Nano Today* **2012,** *7*, 53-65.

72. Choi, K. Y.; Lee, S.; Park, K.; Kim, K.; Park, J. H.; Kwon, I. C.; Jeong, S. Y. Preparation and Characterization of Hyaluronic Acid-Based Hydrogel Nanoparticles. *J. Phys. Chem. Solids* **2008,** *69*, 1591-1595.

73. Sun, Q.; Kang, Z.; Xue, L.; Shang, Y.; Su, Z.; Sun, H.; Ping, Q.; Mo, R.; Zhang, C. A Collaborative Assembly Strategy for Tumor-Targeted siRNA Delivery. *J. Am. Chem. Soc.* **2015,** *137*, 6000-6010.

74. Beldman, T. J.; Senders, M. L.; Alaarg, A.; Pérez-Medina, C.; Tang, J.; Zhao, Y.; Fay, F.; Deichmöller, J.; Born, B.; Desclos, E.; van der Wel, N. N.; Hoebe, R. A.; Kohen, F.; Kartvelishvily, E.; Neeman, M.; Reiner, T.; Calcagno, C.; Fayad, Z. A.; de Winther, M. P. J.; Lutgens, E.; Mulder, W. J. M.; Kluza, E. Hyaluronan Nanoparticles Selectively Target Plaque-Associated Macrophages and Improve Plaque Stability in Atherosclerosis. *ACS Nano* **2017,** *11*, 5785-5799.

75. Potmesil, M., Camptothecins: From Bench Research to Hospital Wards. *Cancer Res.* **1994,** *54*, 1431-1439.

76. Adams, D. J.; Wahl, M. L.; Flowers, J. L.; Sen, B.; Colvin, M.; Dewhirst, M. W.; Manikumar, G.; Wani, M. C. Camptothecin Analogs with Enhanced Activity against Human Breast Cancer Cells. II. Impact of the Tumor pH Gradient. *Cancer Chemother. Pharmacol.* **2006,** *57*, 145-154.

77. Yang, G.; Phua, S. Z. F.; Bindra, A. K.; Zhao, Y. Degradability and Clearance of Inorganic Nanoparticles for Biomedical Applications. *Adv. Mater.* **2019,** *31*, 1805730.

Table of Contents (TOC) Graphic